Properties of human connexin 31, which is implicated in hereditary dermatological disease and deafness

Charles K. Abrams*†‡, Mona M. Freidin*, Vytas K. Verselis*, Thaddeus A. Bargiello*, David P. Kelsell§, Gabriele Richard¶, Michael V. L. Bennett*‡, and Feliksas F. Bukauskas*

Departments of *Neuroscience, and †Neurology, Albert Einstein College of Medicine, 1300 Morris Park Avenue, Bronx, NY 10461; §Centre for Cutaneous Research, Institute for Cell and Molecular Science, Barts and The London School of Medicine and Dentistry, Queen Mary, University of London, 2 Newark Street, Whitechapel, London E1 2AT, United Kingdom; and ¶GeneDx, Inc., 207 Perry Parkway, Gaithersburg, MD 20877

Contributed by Michael V. L. Bennett, January 13, 2006

The connexins are a family of at least 20 homologous proteins in humans that form aqueous channels connecting the interiors of coupled cells and mediating electrical and chemical communication. Mutations in the gene for human connexin 31 (hCx31) are associated with disorders of the skin and auditory system. Alterations in functional properties of Cx31 junctions are likely to play a role in these diseases; nonetheless, little is known about the properties of the wild-type channels. Here we show that hCx31 channels, like other connexin channels, are gated by voltage and close at low pH and when exposed to long-chain alkanols. Single-channel conductance of the fully open channel is ≈85 pS, and it is permeable to Lucifer yellow, Alexa Fluor^{350}, ethidium bromide, and DAPI, which have valences of −2, −1, +1, and +2, respectively. In contrast to what has been reported for mouse Cx31, hCx31 appears to form functional heterotypic channels with all four connexins tested, Cx26, Cx30, Cx32, and Cx45. These findings provide an important first step in evaluating the pathogenesis of inherited human diseases associated with mutations in the gene for Cx31.

electrical coupling | erythrokeratodermia variabilis | gap junction | intercellular communication

The connexins are a family of at least 20 homologous proteins in humans. They form aqueous channels that connect the interiors of coupled cells and mediate electrical and chemical communication. Connexin 31 (Cx31) is one of several connexins associated with human disease (see *Supporting Text*, which is published as supporting information on the PNAS web site, for further details and references). Cx31 is expressed in skin (1, 2), and mutations in the human gene (GJB3) are associated with the genetic skin disorder erythrokeratodermia variabilis (3, 4). Cx31 is also expressed in the mouse cochlea (5, 6) and in peripheral auditory nerves (7), which may explain the association of some mutations in Cx31 with deafness (8). In addition, in a single family with the D66del mutation in Cx31, autosomal dominant peripheral neuropathy has been reported (7). Cx31 is expressed in testis of adults (9), in placenta, and in developing hindbrain (10); however, no abnormalities of these tissues have been reported in patients with mutations in Cx31. Mice with targeted ablation of the gene for Cx31 show transient abnormalities of placental development and reduced viability of homozygous embryos; however, they have no hearing impairment and no skin abnormalities (11).

The X-linked form of Charcot-Marie-Tooth disease (CMTX), associated with mutations in the gene for Cx32 (12), is probably the best studied of the human connexin diseases. Investigations from a number of laboratories suggest that most CMTX-associated mutations lead to a loss of Cx32 function (13). Data suggest this loss of function arises either through defects in trafficking of the mutant protein (14–18) or through alteration of properties of the junctions it forms (19–25). Similarly, studies of human Cx31 (hCx31) suggest that mutations in this connexin may also lead to alterations in trafficking or channel function (26–28), and some mutations increase cell death when expressed in HeLa, NIH 3T3, or NEB1 cells (26, 29). Although mutations in the gene for hCx31 have been associated with autosomal recessive deafness (30) or skin disease (31), most pathogenic hCx31 mutations lead to dominantly inherited disease (3, 4, 30) and are likely to be caused by either toxic gain-of-function or dominant-negative interactions.

Although alterations in functional properties of hCx31 mutants are likely to play a role in human diseases, little is known about the properties of the channels formed by wild-type or mutant forms of this connexin. Here we characterize macroscopic voltage and chemical gating, dye permeability, and single-channel conductance of junctions formed by hCx31. In contrast to the previous report using murine Cx31 (32), hCx31 forms functional heterotypic channels with Cx26, Cx30, Cx32, and Cx45. The findings presented in this communication provide an important benchmark for comparisons with the electrophysiological properties of gap junction channels formed by the mutant forms of Cx31 associated with diseases of the skin and auditory system in human patients.

Results

hCx31 Expression. *Neuro2a* and HeLa cell lines were stably transfected with hCx31–IRES2-EGFP (Cx31WT) or hCx31-EGFP, as described in *Methods*. Expression of mRNAs for Cx31 was confirmed in both *Neuro*2a (Fig. 1*A*) and HeLa cell lines (not shown) using Northern blotting; likewise, protein expression was confirmed by Western blot (Fig. 1*B*). HeLa cells transfected with hCx31WT showed punctate intercellular staining in a pattern consistent with the presence of gap junction plaques (Fig. 1*C*). These puncta had a distribution that was biased to smaller sizes than seen with many other connexins examined in HeLa and *Neuro*2a cells, including Cx32 and Cx43.

hCx31 Voltage and Chemical Gating. Junctional currents were recorded in response to transjunctional voltage steps (Fig. 1*D*) in isolated pairs of *Neuro*2a cells expressing Cx31 and HeLa cells expressing Cx31-EGFP. As for most other homotypic junctions formed of connexins, the rate and degree of decay of junctional currents increased as a function of the transjunctional voltage, V_j of either sign. The steady-state conductance, g_j (or G_j when normalized to the value at $V_j = 0$), showed a maximum at $V_j = 0$ and declined symmetrically for V_j of either sign to a minimum value of ≈0.25 (Fig. 1*E*). Residual conductance, G_{jmin}, at large voltages reflects closure to a substate conductance. No differences were noted in voltage dependence between hCx31 and hCx31-EGFP. Boltzmann parameters were determined from these relations and are listed in the legend for Fig. 1. We evaluated the response of the hCx31 channels to heptanol and

Conflict of interest statement: No conflicts declared.

Abbreviations: Cx, connexin; hCx, human Cx; EtdBr, ethidium bromide.

‡To whom correspondence may be addressed. E-mail: cabrams@aecom.yu.edu or mbennett@aecom.yu.edu.

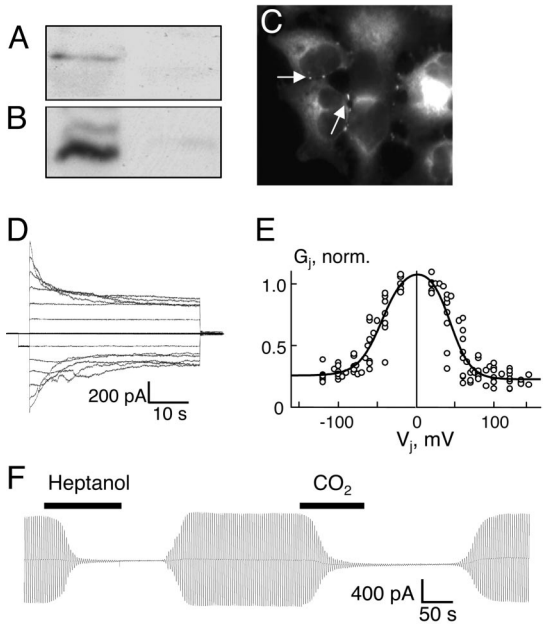

Fig. 1. Expression and gating of hCx31. (*A*) Northern blot analysis of mRNA extracts from a *Neuro*2a cell line expressing hCx31 (left lane) and wild-type HeLa cells (right lane). (*B*) Western blot analysis of protein extracts from a *Neuro*2a cell line expressing hCx31 (left lane) and parental HeLa cells (right lane). (*C*) Immunostaining for hCx31WT expressed in HeLa cells shows punctate staining in a pattern consistent with the presence of gap junction plaques (arrows). (*D*) Representative current traces in response to V_j steps for homotypic hCx31 junctions between a pair of transfected *Neuro*2a cells. Both cells were voltage-clamped at 0 mV, junctional currents were recorded from cell 2, and cell 1 was stepped to voltages from zero to ±120 mV in increments of 20 mV. A 0.5-s +20-mV standardizing pulse step preceded each test pulse. (*E*) G_j–V_j relation for homotypic hCx31 channels between transfected *Neuro*2a cells. Each circle in the G_j–V_j plot is derived from a single determination of steady-state current. The solid line represents fits of the data to Boltzmann distributions for V_j of either sign. Parameters ($+V_j$, $-V_j$); G_{min}, 0.24, 0.21; G_{max}, 1.1, 1.1; A, 0.065, 0.076; V_0, 43.8, 43.9. (*F*) Chemical gating and pH sensitivity of hCx31 channels between HeLa cells. I_j was measured during application of repeated V_j ramps from −22 to +22 mV every 1.5 s. Application of 2 mM heptanol led to a rapid reduction in junctional current to below detectable levels. Junctional current rapidly recovered when heptanol was removed from the bath. Application of CO_2 saturated bath solution also caused rapid and reversible reduction in I_j.

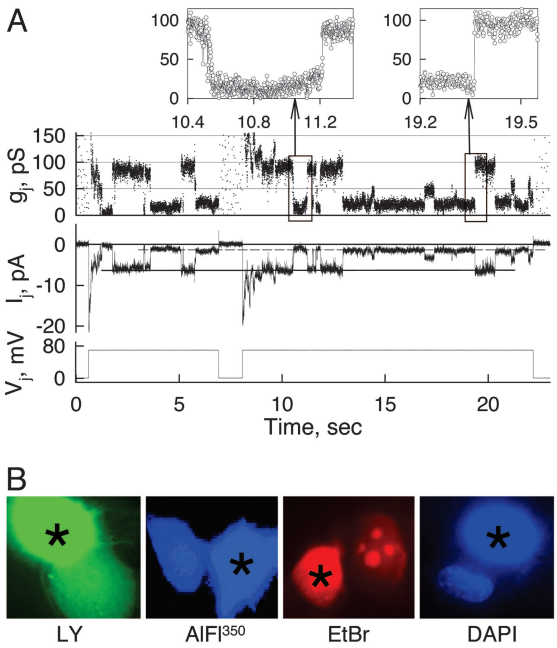

Fig. 2. Single-channel conductance and permeability of hCx31-EGFP channels measured in HeLa cells. (*A*) Junctional current records (middle trace) in response to voltage steps (bottom trace) from 0 to +70 mV. The dashed line on the current record is the residual conductance; the solid line is the fully open state of one channel. A point-by-point (1-ms) calculation of the junctional conductance is shown in the top row (g_j). The conductance of the fully open channel is ≈85 pS, and a predominant residual conductance of ≈15 pS is seen. Two *Insets* on the top show expanded records from regions defined by rectangles and illustrate the slow gating transition from the open state toward the closed state (*Left Inset*) and the fast gating transition from the substate to the open state (*Right Inset*). (*B*) Permeability of hCx31 junctions to fluorescent dyes. Cell 1 (asterisk) was loaded with the dye of interest via the patch pipette in the whole-cell recording configuration, and a gigaohm seal (on cell configuration) with cell 2 was established via a second patch pipette. In this way, the dye that crossed into cell 2 (the postjunctional cell) was not lost by diffusion into pipette 2. After a suitable interval (usually 5 min), the gigaohm seal on cell 2 was ruptured, g_j measured, and the presence of a cytoplasmic bridge excluded by application of 2 mM heptanol. As shown here, hCx31 is relatively nonselective, allowing passage of both negatively and positively charged dyes including Lucifer yellow (LY, −2), Alexa Fluor^{350} (AF^{350}, −1), EtdBr (+1), and DAPI (+2).

to intracellular acidification by bath application of solution saturated with 100% CO_2 (Fig. 1*F*). Both heptanol- and acidification-induced rapid and reversible closure of the cell–cell channels formed by hCx31.

hCx31 Channel Conductance and Permeability. Although most cell pairs expressed junctional conductances too large to observe unitary current events, we could see single-channel activity during recovery from CO_2 or heptanol-induced reduction in junctional conductance, g_j. The middle record of Fig. 2*A* shows the junctional currents (I_j) resulting from the application of V_j steps (bottom record) to one of two HeLa cells expressing hCx31-EGFP. There were multiple active intercellular channels, determined from the I_j and g_j records and the rapid closing at the onset of the V_j steps from 0 to +70 mV. Subsequent to the initial rapid decrease, there were several further unitary transitions during the V_j steps. The g_j record (Fig. 2*A Upper*) shows that the conductance of the fully open channel was ≈85 pS. There were rapid transitions of ≈70 pS (see Fig. 2*A Inset* on the top right, in which open circles show the conductance at successive 1-ms intervals) to a prominent residual state (dashed line on I_j record) and from the residual state to the fully open state (in expanded sweeps). Less frequently, we observed slow gating transitions between the fully open and fully closed states. Fig. 2*A Inset* on the top left shows a slow gating transition from the open state toward the closed state with two brief interruptions in which g_j returned toward the open state. g_j was stable at ≈15 pS for ≈200 ms, slowly decreased, increased again, and then returned to the fully open state. The conductance of the residual state was ≈15 pS, but this value is uncertain, because the number of channels occupying this state was not clear. Findings in cells expressing hCx31 not fused to EGFP were similar (not shown). In the interval from 14 to 22 s, there are slow transitions in and out of a ≈30 pS state that can be attributed to endogenous Cx45 channels (33).

To assess permeability, we measured dye transfer and g_j in isolated HeLa cell pairs expressing hCx31 or hCx31-EGFP, as described in *Methods*. Measurement of coupling in the same cell pairs and showing that it could be blocked by heptanol allowed us to exclude false negatives due to the lack of coupling and false positives due to the presence of cytoplasmic bridges. Each dye was examined at least in five experiments. As shown in Fig. 2*B*, hCx31 channels are permeable to Lucifer yellow, Alexa Fluor^{350}, ethidium bromide (EtdBr), and DAPI, which have valences of

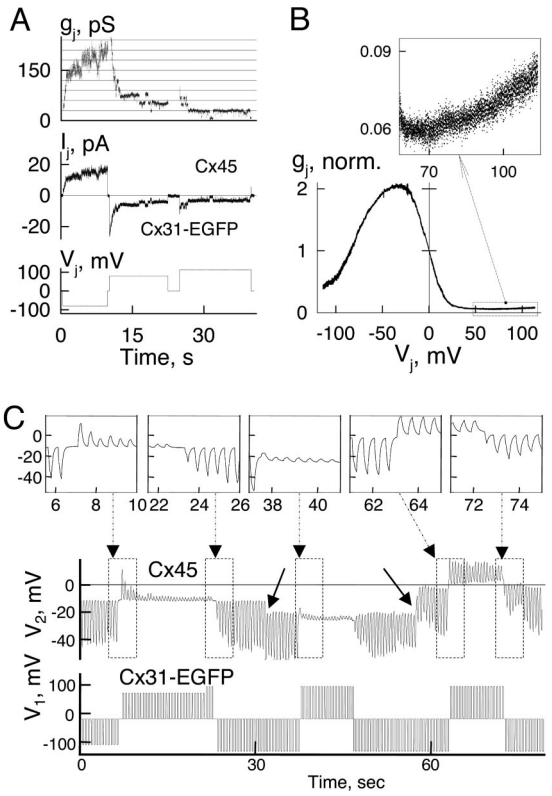

Fig. 3. hCx31 forms heterotypic junctions with Cx45. (*A*) The bottom trace shows the voltage applied to a HeLa cell expressing hCx31-EGFP and paired with a HeLa cell expressing Cx45 voltage clamped at 0. The middle trace shows the junctional currents measured in the cell expressing Cx45. The top trace shows g_j calculated point by point. These heterotypic junctions have a markedly asymmetric response to V_j. (*B*) Steady-state G_j–V_j relation for Cx45/Cx31-EGFP heterotypic junctions assembled from slow (4 min) ramps from 0 to +100 mV and from 0 to −100 mV. For increasing negativity on the hCx31-EGFP side, G_j increases up to ≈40 mV before decreasing again. For V_j of the opposite polarity, G_j decreases to a minimum at approximately −60 mV (*Inset*) and then shows a small increase. (*C*) Dependence of heterotypic Cx45/Cx31-EGFP coupling on holding current. A hCx31-EGFP-expressing cell (cell 1) was voltage-clamped at −10 mV and stepped by ±90 mV for 0.25 s with 0.25 s between pulses, and a coupled Cx45-expressing cell (cell 2) was current-clamped to approximately −12 mV. Hyperpolarizing voltage pulses starting before the record shown were applied to the hCx31-EGFP cell; these pulses caused g_j to increase, and there was a substantial response in cell 2. After ≈5 s, the pulses were changed to depolarizing, and the responses in cell 2 decreased gradually with successive pulses, indicating decrease in g_j. Expanded records in the *Insets* above show the changes associated with change in polarity in greater detail. Reapplication of hyperpolarizing pulses to cell 1 caused the responses in cell 2 to increase again, indicating increased g_j. At ≈30 s, the hyperpolarizing current in cell 2 was increased; the responses to hyperpolarizing steps in cell 1 remained about the same, but the responses to depolarizing steps were greatly reduced. At ≈58 s, the hyperpolarizing current in cell 2 was decreased below the initial value, and the responses to depolarization and hyperpolarization of cell 1 were of more nearly the same amplitude.

−2, −1, +1, and +2, respectively. Based on these data, the channels appear to be relatively permeable to large ions and not selective on the basis of charge.

hCx31 Forms Heterotypic Junctions. To determine whether hCx31 forms heterotypic cell–cell channels with Cx45, we cocultured HeLa cells stably expressing rCx45 and with cells expressing hCx31-EGFP. Cells pairs were selected based on expression of hCx31-EGFP hemiplaques by one cell. As shown in Fig. 3 *A* and *B*, hCx31-EGFP formed heterotypic junctions with Cx45; the quasisteady-state G_j–V_j relation in Fig. 3*B* (obtained by application of a slow voltage ramp) shows closure on both polarities of V_j. Cx45 has previously been reported to gate with negative polarity, i.e., the gate that closes is in the hemichannel on the relatively negative side (33); the findings here are consistent with both Cx45 and hCx31 closing with negative gating polarity. The Cx45/Cx31-EGFP steady-state G_j–V_j relationship is highly asymmetric. Specifically, G_j decreases for V_j pulses $< \approx 40$ mV, which make the cell expressing hCx31-EGFP relatively positive and increases for equal V_j pulses that make that cell relatively negative. Several factors contribute to the asymmetry. First, the steady-state G_j–V_j relation for homotypic hCx31 junctions (Fig. 1) is much less sensitive to V_j than that for Cx45 junctions (33). Second, the conductance of a single hCx31 hemichannel, ≈160 pS based on the assumption that it is twice that of a cell–cell channel, is ≈3 times that of a Cx45 hemichannel, 57 pS (34). Thus, a larger fraction of an applied V_j is developed across the Cx45 hemichannel, thereby increasing its sensitivity to V_j. Third, the increase in g_j between 0 and −40 mV is ascribable to a relatively low open probability of the Cx45 hemichannel at V_j = 0 (≈0.5). As V_j on the hCx31 side is made more negative, the open probability of the hCx31 hemichannel remains ≈1.0 at small negative voltages, and the open probability of the Cx45 hemichannels and g_j increase. As negativity on the hCx31 side increases beyond ≈40 mV, the hCx31 hemichannel tends to close, and g_j decreases. Fourth, there is a small increase in g_j for large positivity on the hCx31 side (Fig. 3*B Inset* with higher sensitivity for g_j). We ascribe this secondary increase to occasional opening of the slow gate of the Cx45 hemichannel followed by rapid closing of its fast gate to the residual conductance (33).

Because of the markedly asymmetric and highly sensitive voltage dependence of Cx45/Cx31-EGFP junctions at small V_j, transmission of voltage steps across the junctions shows marked asymmetry and dependence on small differences in holding potentials. For Fig. 3*C* from a heterotypic Cx45/Cx31-EGFP cell pair, the Cx45 cell was current-clamped and polarized to −12 mV, and the hCx31-EGFP cell was voltage-clamped at −10 mV and repetitively stepped to −100 or +80 mV for 0.2 s and then to −10 mV for 0.3 s. At the beginning of the record, negative pulses on the hCx31-EGFP side, which tended to increase g_j (see Fig. 3*B*), caused pulses attenuated by approximately two-thirds in the Cx45 cell. Positive pulses, equivalent to applying a mean positive voltage on the hCx31-EGFP side because the time constant of changes in g_j, are longer than the duty cycle of the pulses, caused a decrease in g_j over several seconds and greatly decreased the amplitude of the responses in the Cx45 cell. When the pulses on the hCx31-EGFP side were again made negative, the responses in the Cx45 cell gradually increased again as g_j increased. (The amplitude of the voltage-clamp pulses was increased by ≈15 mV ≈3 s before the reversal of polarity.) Fig. 3*C Insets* show, with better time resolution, the responses in the Cx45 cell associated with change in polarity of the pulses in the hCx31-EGFP cell. The degree of asymmetry in the responses in the Cx45 expressing cell was very sensitive to V_j. At the first solid arrow, the holding current in the Cx45 cell was adjusted to change its baseline membrane potential from about −12 to −20 mV; at the second solid arrow, the baseline potential was changed to −2 mV. Making the Cx45 cell more negative (to −20 mV) increased the rate of decay for positive pulses but had little effect on the steady-state responses. Making the Cx45 cell more positive (to −2 mV) increased coupling for positivity on the hCx31-EGFP side and made the responses more symmetrical. These findings are similar to those obtained from Cx45/Cx43 heterotypic junctions (33).

hCx26, hCx30, and hCx32 also form functional heterotypic gap junctions with hCx31 (Figs. 4 and 5). Heterotypic junctions formed by Cx32 and hCx31 close on both polarities of V_j, as follows from the steady-state G_j–V_j plot (Fig. 4*B*, filled squares).

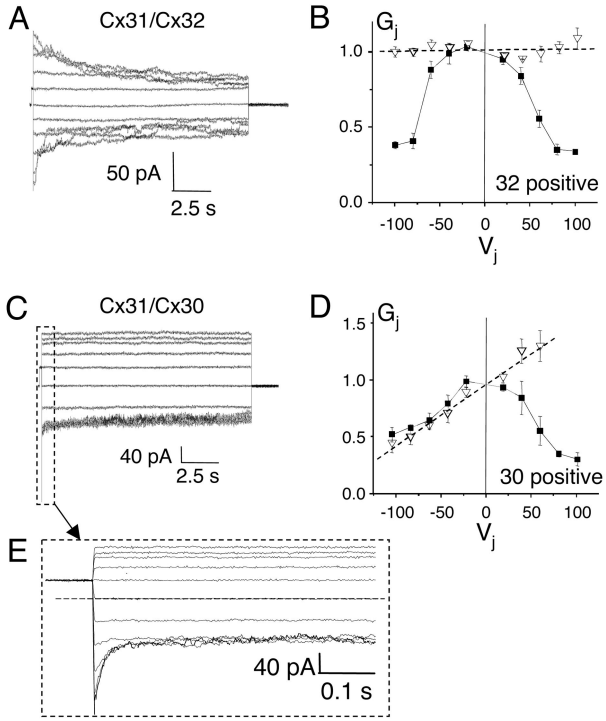

Fig. 4. hCx31 forms heterotypic junctions with Cx32 and Cx30. Representative I_j traces in response to V_j steps (*A* and *C*) and average normalized G_j–V_j relations (*B* and *D*) for hCx31 paired heterotypically with Cx32 and Cx30. (*A* and *C*) Both cells were voltage-clamped at 0 mV, and cell 1 (expressing Cx32 or Cx30) was stepped to −20 mV for 0.2 s for normalization and then to voltages between +100 and −100 mV in 20-mV increments and I_j recorded from the hCx31-expressing cell. (*B* and *D*) Instantaneous (open triangles) and steady-state (filled squares) G_j–V_j relations for each cell pair. The dashed lines represent best fit straight lines for the instantaneous g_j). (*E*) An expanded view of the first 500 ms of traces in *C*. The dashed line is at $I_j = 0$.

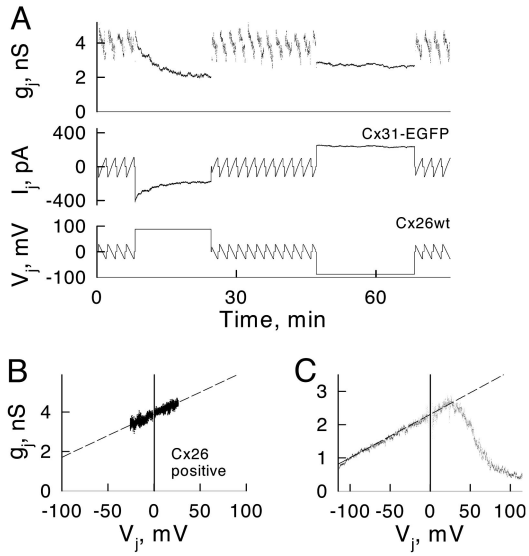

Fig. 5. hCx31 forms heterotypic junctions with Cx26. (*A*) I_j record (middle trace) from a hCx31-EGFP/Cx26 heterotypic cell pair in response to V_j ramps and steps applied to a cell expressing Cx26 (bottom trace). The corresponding junctional conductances are shown in the upper trace. I_j in response to a positive step declined to steady state over ≈15 s; fast g_j recovery measured during repeated V_j ramps after a positive V_j step indicates that the fast gating mechanism was responsible for this g_j decay. During a negative V_j step, g_j decayed instantaneously by ≈25% and remained relatively constant. The small ramps caused rapid changes in g_j (see *B*). (*B*) Changes in g_j induced by the small ramps decaying from +28 to −28 mV every 2 s; g_j increases quite linearly with voltage over that voltage range. The dashed line is a linear fit to the data. (*C*) Steady-state G_j–V_j relation for a hCx31-EGFP/Cx26 heterotypic cell pair assembled from slow (4 min) ramps from 0 to +100 mV and from 0 to −100 mV. The dashed line represents the linear fit of data points at V_js from −110 to +15 mV.

Because Cx32 closes on negativity (35), this finding confirms that hCx31 also closes on negativity, as it does in Cx45/Cx31 junctions. hCx31/Cx32 heterotypic junctions show no well expressed instantaneous rectification (Fig. 4 *A* and *B*, open triangles); the steady-state G_j–V_j relation is somewhat asymmetric (Fig. 4*B*), with the limb referable to gating by the hCx31 hemichannel (positive on the Cx32 side) showing a greater V_j sensitivity than the limb for Cx32.

The steady-state conductance of hCx31/Cx30 junctions is decreased when the cell expressing Cx30 is pulsed positive, making V_j negative with respect to the cell expressing hCx31; there is a more or less linear decrease in g_j for the opposite polarity of V_j (Fig. 4*C*, expanded time scale in *E*, graph in *D*). The data for hCx32/hCx30 junctions are consistent with the negative gating polarity of hCx31 inferred here, the positive gating polarity of rCx30 (36), and the positive gating polarity of hCx30 when paired with hCx32 or hCx26 (C.K.A., unpublished work). Therefore, both Cx30 and hCx31 hemichannels tend to close at positive V_js. The decrease for the Cx30 side negative and the hCx31 side positive is ascribable to ''instantaneous'' rectification of single open-channel currents. The initial currents show an ≈3-fold rectification between −100 and +60 mV (Fig. 4 *C*–*E*); very rapid gating made determination of instantaneous rectification at larger positive potentials difficult, but extrapolation predicts ≈3.75-fold rectification between −100 and +100 mV. This degree of rectification is similar to that seen with human hCx32/hCx30 junctions (C.K.A., unpublished work) and hCx32/hCx26 (C.K.A., unpublished work) or hCx32/rCx26 junctions (37).

The g_j–V_j relations of hCx31/Cx26 junctions were examined by using voltage ramps in addition to voltage steps and showed slow changes ascribable to gating for negativity on the hCx31 side and positivity on the Cx26 side (Fig. 5 *A* and *C*); these changes are consistent with negative gating polarity of hCx31 and positive gating polarity for Cx26 (35). However, most of the applied V_j would be across the hCx31 hemichannel in these junctions, because the hCx31 cell–cell channel has a much smaller conductance than the Cx26 channel (38). Thus, the polarity of V_j gating of Cx26 cannot be inferred from the data here. Small and relatively fast ramps showed currents ascribable to (instantaneous) rectification of open single channels with increasing conductance for negativity on the hCx31 side (Fig. 5 *A* and *B*). The conductance voltage relation taken from the small ramps showed an ≈1.4-fold rectification between −30 and +30 mV (Fig. 5*B*); a larger slow ramp showed nearly linear rectification between −110 and +30 mV. If linearly extrapolated to −/+100 mV, both experiments show nearly the same rectification with ≈3.6-fold change of g_j.

Discussion

In this report, we describe the functional properties of the cell–cell channel formed by hCx31 expressed in stably transfected *Neuro*2a and HeLa cell lines. Junctions formed by hCx31 show a symmetric macroscopic G_j–V_j relation similar to that reported for the related connexin, Cx32. Studies of the gating of single hCx31 channels suggest that in the homotypic configuration, gating is dominated by the fast gating mechanism to the residual state. This is in agreement with the macroscopic currents for which the ratio of g_{jmin} to g_{jmax} is ≈0.2 (see Fig. 1 *D* and *E*). g_{jmin}/g_{jmax} is nearly the same as $\gamma_{res}/\gamma_{open}$, the ratio of the

single-channel conductance of the residual state to that of the fully open state (15 pS/85 pS = 0.18).

The single-channel conductance of ≈85 pS for the fully open state is close to that for Cx32. hCx31 is relatively nonselective, allowing passage of large monovalent and divalent cations and anions. The dye transfer studies extend those previously performed on mouse Cx31 (32), showing only LY, DAPI, and neurobiotin cell-to-cell transfer and on hCx31 showing 6-carboxyfluorescein (27) and Alexa Fluor^{568} (26) cell-to cell transfer. mCx31 gap junction channels were reported to lack permeability to EtdBr (32), whereas here we demonstrate that hCx31 junctions are permeable to EtdBr (see Fig. 2). However, the lower sensitivity of the technique used in the earlier study may have made it difficult to observe transfer of EtdBr, because EtdBr tends to bind strongly to nuclei and may be largely trapped in the injected cell. The mouse and hCx31 sequences differ somewhat, most prominently in their N and C termini. However, the possible impact of these differences on permeability will require further study.

Our studies indicate that hCx31 can form heterotypic channels with Cx26, Cx30, Cx32, and Cx45. In contrast, Elfgang *et al.* (32) observed no heterotypic coupling by Cx31. Although they worked with murine Cx31 and examined dye transfer, we used hCx31 and measured electrical coupling, the latter being a more sensitive technique. The patterns of instantaneous rectification for Cx31/Cx26 and Cx31/Cx30 heterotypic junctions are qualitatively similar to those for Cx32/Cx26 and Cx32/Cx30, which suggests that the overall charge distribution within the Cx31 pore is similar to that of Cx32. However, differences likely exist between the charge distributions for hCx31 and Cx32, because hCx31 is permeable to DAPI, a divalent cation, whereas Cx32 is not (39).

Coupling between Cx31 and Cx26, Cx32, or Cx45 may be important for both the development and function of a number of tissues. In humans, Cx31 is expressed in the suprabasal layer of palmar and interfollicular epidermis; the expression is greater in stratum granulosum than in stratum spinosum (2). The distribution of Cx26 overlaps with that of Cx31 in the stratum granulosum of palmar epidermis, although interfollicular epidermis shows little staining for Cx26. Cx30 and Cx45 were also noted in the suprabasal layers of palmar epidermis, especially in stratum granulosum (2). An earlier report (1) identified Cx31, Cx26, and Cx45 in embryonic mouse skin but found only Cx31 in the adult. A recent report by Di *et al.* (40) suggests that Cx31 can form heteromeric hemichannels with Cx26 or Cx30, greatly expanding the potential types of cell–cell channels that may be produced when these connexins are coexpressed in epidermal cells and allowing for transdominant negative actions of mutants.

Interactions between Cx31 and Cx45 may occur during early development. *Xenopus* Cx31 and Cx43.4, the orthologues of hCx31 and Cx45, are expressed in both oocytes and early embryos (41). Cx31 and Cx45 transcripts occur in the pronucleate to four cell stage during human embryogenesis (42). Thus, heterotypic coupling between Cx31 and Cx45 may be important in early stages of development. As shown above, small differences in the resting potentials of two cells coupled by Cx31/Cx45 junctions may dramatically influence the degree of chemical and electrical coupling; positivity on Cx45 side significantly increases and negativity decreases cell–cell coupling.

mRNA transcripts for Cx26 and Cx31 (and six other connexins) are present in central rat cornea, whereas peripheral rat cornea expresses these eight and four additional connexin transcripts, including Cx30 and Cx45 (43). Cx26, Cx30, and Cx31 are expressed in human cochlea, but the pattern of expression of Cx31 differs from those of the other two connexins (5, 6). Cx31 and Cx32 mRNA are expressed in overlapping distributions in developing mouse cochlea (44).

As described above, Cx31 is expressed in a number of different tissues and at different times during development in non-human organisms. Until now, mutations in hCx31 have been clearly identified as etiologic only in deafness and in skin disorders. Most disease-causing mutations in the gene for Cx31 are dominant, although examples of recessive inheritance have been reported (45). Further analysis of the functional properties may help to explain why these mutations do not have clinical effects on the majority of the tissues in which they are expressed.

Methods

Cloning, Transfection, Immunofluorescence, and Western and Northern Blotting. DNA for hCx31, hCx26, hCx30, hCx32, and mouse Cx45 was amplified by PCR from human or mouse genomic DNA, cloned into PGEM-7zf (Promega), sequenced, and subcloned into pIRES2-EGFP (BD Biosciences, Palo Alto, CA). Oligonucleotide-directed PCR-based mutagenesis was used to change the stop codon of Cx31 to Val and of Cx32 to Gly. The resulting PCR products were ligated into pEGFP-N3 or pEYFP-N1 (BD Biosciences), respectively. HeLa or *Neuro*2a cells were transfected by using Lipofectin, and stable cell lines were selected as described in Abrams *et al.* (46). Western blots were incubated 2 h with polyclonal antibodies to Cx31 (2). For Northern blotting, total RNA was extracted from Neuro2a cells grown to 80% confluence. Northern blotting was performed by using the Northern-max-Gly kit (Ambion, Austin, TX). Blots were probed with a full-length antisense RNA probe to hCx31 and labeled with psoralen-biotin using the Brightstar labeling kit (Ambion).

Electrophysiology and Fluorescence Imaging. Dual whole-cell patch clamping was performed as described (47). Cell pairs forming heterotypic junctions were selected based on EGFP fluorescence pattern or by staining cells expressing wild-type connexins with Vybrant 1,1′-dioctadecyl-3,3,3′,3′-tetramethylindocarbocyanine dye. Fluorescence signals were recorded and analyzed by using the UltraVIEW imaging system (Perkin-Elmer). Intercellular dye transfer was measured after loading one cell with dye through the patch pipette and monitoring the dynamics of fluorescence intensity in both cells of the pair. Dyes used include [M_r of the ion, valence: Lucifer yellow (443, −2), Alexa Fluor^{350} (350, −1), EtdBr (314, +1), and DAPI (279, +2).

Expanded methods are in *Supporting Text*.

We thank Angele Bukauskiene for outstanding technical assistance and Fatima Rouan for providing the Cx31-EGFP vector. This work was supported by National Institutes of Health Grants K08-NS02149 and K02-NS050345 (to C.K.A.), NS45287 (to M.V.L.B.), R01 NS036706 (to F.F.B.), and K08-AR02141 (to G.R.); by the F. M. Kirby Program in Neural Repair and Protection of the Albert Einstein College of Medicine; and by the Biotechnology and Biological Sciences Research Council (to D.P.K.). M.V.L.B. is the Sylvia and Robert S. Olnick Professor of Neuroscience.

1. Butterweck, A., Elfgang, C., Willecke, K. & Traub, O. (1994) *Eur. J. Cell Biol.* **65,** 152–163.
2. Di, W. L., Rugg, E. L., Leigh, I. M. & Kelsell, D. P. (2001) *J. Invest. Dermatol.* **117,** 958–964.
3. Richard, G., Smith, L. E., Bailey, R. A., Itin, P., Hohl, D., Epstein, E. H., Jr., DiGiovanna, J. J., Compton, J. G. & Bale, S. J. (1998) *Nat. Genet.* **20,** 366–369.
4. Richard, G., Brown, N., Smith, L. E., Terrinoni, A., Melino, G., Mackie, R. M., Bale, S. J. & Uitto, J. (2000) *Hum. Genet.* **106,** 321–329.
5. Xia, A. P., Ikeda, K., Katori, Y., Oshima, T., Kikuchi, T. & Takasaka, T. (2000) *NeuroReport* **11,** 2449–2453.
6. Forge, A., Becker, D., Casalotti, S., Edwards, J., Marziano, N. & Nevill, G. (2003) *J. Comp. Neurol.* **467,** 207–231.

7. Lopez-Bigas, N., Olive, M., Rabionet, R., Ben-David, O., Martinez-Matos, J. A., Bravo, O., Banchs, I., Volpini, V., Gasparini, P., Avraham, K. B., *et al.* (2001) *Hum. Mol. Genet.* **10,** 947–952.
8. Rabionet, R., Lopez-Bigas, N., Arbones, M. L. & Estivill, X. (2002) *Trends Mol. Med.* **8,** 205–212.
9. Plum, A., Hallas, G. & Willecke, K. (2002) *Genomics* **79,** 24–30.
10. Jungbluth, S., Willecke, K. & Champagnat, J. (2002) *Dev. Dyn.* **223,** 544–551.
11. Plum, A., Winterhager, E., Pesch, J., Lautermann, J., Hallas, G., Rosentreter, B., Traub, O., Herberhold, C. & Willecke, K. (2001) *Dev. Biol.* **231,** 334–347.
12. Bergoffen, J., Scherer, S. S., Wang, S., Scott, M. O., Bone, L. J., Paul, D. L., Chen, K., Lensch, M. W., Chance, P. F. & Fischbeck, K. H. (1993) *Science* **262,** 2039–2042.
13. Abrams, C., Oh, S., Ri, Y. & Bargiello, T. (1999) *Brain. Res. Brain. Res. Rev.* **32,** 203–214.
14. Deschenes, S. M., Walcott, J. L., Wexler, T. L., Scherer, S. S. & Fischbeck, K. H. (1997) *J. Neurosci.* **17,** 9077–9084.
15. Kleopa, K. A., Yum, S. W. & Scherer, S. S. (2002) *J. Neurosci. Res.* **68,** 522–534.
16. Matsuyama, W., Nakagawa, M., Moritoyo, T., Takashima, H., Umehara, F., Hirata, K., Suehara, M. & Osame, M. (2001) *J. Hum. Genet.* **46,** 307–313.
17. Martin, P. E., Mambetisaeva, E. T., Archer, D. A., George, C. H. & Evans, W. H. (2000) *J. Neurochem.* **74,** 711–720.
18. Yum, S. W., Kleopa, K. A., Shumas, S. & Scherer, S. S. (2002) *Neurobiol. Dis.* **11,** 43–52.
19. Abrams, C. K., Bennett, M. V. L., Verselis, V. K. & Bargiello, T. A. (2002) *Proc. Natl. Acad. Sci. USA* **99,** 3980–3984.
20. Bruzzone, R., White, T. W., Scherer, S. S., Fischbeck, K. H. & Paul, D. L. (1994) *Neuron* **13,** 1253–1260.
21. Oh, S., Ri, Y., Bennett, M. V. L., Trexler, E. B., Verselis, V. K. & Bargiello, T. A. (1997) *Neuron* **19,** 927–938.
22. Omori, Y., Mesnil, M. & Yamasaki, H. (1996) *Mol. Biol. Cell* **7,** 907–916.
23. Ressot, C., Gomes, D., Dautigny, A., Pham-Dinh, D. & Bruzzone, R. (1998) *J. Neurosci.* **18,** 4063–4075.
24. Wang, H. L., Chang, W. T., Yeh, T. H., Wu, T., Chen, M. S. & Wu, C. Y. (2004) *Neurobiol. Dis.* **15,** 361–370.
25. Yoshimura, T., Satake, M., Ohnishi, A., Tsutsumi, Y. & Fujikura, Y. (1998) *J. Neurosci. Res.* **51,** 154–161.
26. Di, W. L., Monypenny, J., Common, J. E., Kennedy, C. T., Holland, K. A., Leigh, I. M., Rugg, E. L., Zicha, D. & Kelsell, D. P. (2002) *Hum. Mol. Genet.* **11,** 2005–2014.
27. Rouan, F., Lo, C. W., Fertala, A., Wahl, M., Jost, M., Rodeck, U., Uitto, J. & Richard, G. (2003) *Exp. Dermatol.* **12,** 191–197.
28. Diestel, S., Eckert, R., Hulser, D. & Traub, O. (2004) *Exp. Cell Res.* **294,** 446–457.
29. Diestel, S., Richard, G., Doring, B. & Traub, O. (2002) *Biochem. Biophys. Res. Commun.* **296,** 721–728.
30. Liu, X. Z., Xia, X. J., Xu, L. R., Pandya, A., Liang, C. Y., Blanton, S. H., Brown, S. D., Steel, K. P. & Nance, W. E. (2000) *Hum. Mol. Genet.* **9,** 63–67.
31. Gottfried, I., Landau, M., Glaser, F., Di, W. L., Ophir, J., Mevorah, B., Ben-Tal, N., Kelsell, D. P. & Avraham, K. B. (2002) *Hum. Mol. Genet.* **11,** 1311–1316.
32. Elfgang, C., Eckert, R., Lichtenberg-Frate, H., Butterweck, A., Traub, O., Klein, R. A., Hulser, D. F. & Willecke, K. (1995) *J. Cell Biol.* **129,** 805–817.
33. Bukauskas, F. F., Angele, A. B., Verselis, V. K. & Bennett, M. V. L. (2002) *Proc. Natl. Acad. Sci. USA* **99,** 7113–7118.
34. Valiunas, V. (2002) *J. Gen. Physiol.* **119,** 147–164.
35. Verselis, V. K., Ginter, C. S. & Bargiello, T. A. (1994) *Nature* **368,** 348–351.
36. Dahl, E., Manthey, D., Chen, Y., Schwarz, H. J., Chang, Y. S., Lalley, P. A., Nicholson, B. J. & Willecke, K. (1996) *J. Biol. Chem.* **271,** 17903–17910.
37. Barrio, L. C., Suchyna, T., Bargiello, T., Xu, L. X., Roginski, R. S., Bennett, M. V. L. & Nicholson, B. J. (1991) *Proc. Natl. Acad. Sci. USA* **88,** 8410–8414.
38. Bukauskas, F. F., Elfgang, C., Willecke, K. & Weingart, R. (1995) *Pflügers Arch.* **429,** 870–872.
39. Trexler, E. B., Bukauskas, F. F., Kronengold, J., Bargiello, T. A. & Verselis, V. K. (2000) *Biophys. J.* **79,** 3036–3051.
40. Di, W. L., Gu, Y., Common, J. E., Aasen, T., O'Toole E., A., Kelsell, D. P. & Zicha, D. (2005) *J. Cell. Sci.* **118,** 1505–1514.
41. Landesman, Y., Postma, F. R., Goodenough, D. A. & Paul, D. L. (2003) *J. Cell. Sci.* **116,** 29–38.
42. Bloor, D. J., Wilson, Y., Kibschull, M., Traub, O., Leese, H. J., Winterhager, E. & Kimber, S. J. (2004) *Reprod. Biol. Endocrinol.* **2,** 25.
43. Laux-Fenton, W. T., Donaldson, P. J., Kistler, J. & Green, C. R. (2003) *Cornea* **22,** 457–464.
44. Lopez-Bigas, N., Arbones, M. L., Estivill, X. & Simonneau, L. (2002) *Gene. Expr. Patterns* **2,** 113–117.
45. Richard, G. (2003) *Clin. Exp. Dermatol.* **28,** 397–409.
46. Abrams, C. K., Freidin, M., Bukauskas, F., Dobrenis, K., Bargiello, T. A., Verselis, V. K., Bennett, M. V. L., Chen, L. & Sahenk, Z. (2003) *J. Neurosci.* **23,** 10548–10558.
47. Bukauskas, F. F., Jordan, K., Bukauskiene, A., Bennett, M. V. L., Lampe, P. D., Laird, D. W. & Verselis, V. K. (2000) *Proc. Natl. Acad. Sci. USA* **97,** 2556–2561.